Hindawi
Geofluids
Volume 2021, Article ID 5595277, 16 pages
https://doi.org/10.1155/2021/5595277

Research Article

Application of GA-BP Neural Network Optimized by Grey Verhulst Model around Settlement Prediction of Foundation Pit

C. Y. Liu, Y. Wang, X. M. Hu, Y. L. Han, X. P. Zhang, and L. Z. Du

College of Construction and Engineering, Jilin University, Changchun 130000, China

Correspondence should be addressed to X. P. Zhang; xiaopei@jlu.edu.cn and L. Z. Du; dulizhi98@jlu.edu.cn

Received 6 January 2021; Revised 31 January 2021; Accepted 13 February 2021; Published 4 March 2021

Academic Editor: Feng Xiong

Due to the limitation in the prediction of the foundation pit settlement, this paper proposed a new methodology which takes advantage of the grey Verhulst model and a genetic algorithm. In the previous study, excavation times are often the only factor to predict the settlement, which is mainly because the correspondence between real-time excavation depth and the excavation time is hard to determine. To solve this issue, the supporting times are precisely recorded and the excavation depth rate can be obtained through the excavation time length and excavation depth between two adjacent supports. After the correspondence between real-time excavation depth and the excavation time is obtained, the internal friction angle, cohesion, bulk density, Poisson's ratio, void ratio, water level changes, permeability coefficient, number of supports, and excavation depth, which can influence the settlement, are taken to be considered in this study. For the application of the methodology, the settlement monitoring point of D4, which is near the bridge pier of the highway, is studied in this paper. The predicted values of the BP neural network, GA-BP neural network, BP neural network optimized by the grey Verhulst model, and GA-BP neural network optimized by the grey Verhulst model are detailed compared with the measured values. And the evaluation indexes of RMSE, MAE, MSE, MAPE, and R^2 are calculated for these models. The results show that the grey Verhulst model can greatly improve the consistency between predicted values and measured values, while the accuracy and resolution is still low. The genetic algorithm (GA) can greatly improve the accuracy of the predicted values, while the GA-BP neural network shows low reflection to the fluctuation of measured values. The GA-BP neural network optimized by the grey Verhulst model, which has taken the advantages of GA and the grey Verhulst model, has extremely high accuracy and well consistency with the measured values.

1. Introduction

In recent years, China's engineering construction has developed rapidly, especially for deep foundation pit projects, caused by the need of large-scale public facilities and lots of exploitation of underground spaces [1–9]. However, the settlement of the foundation pit is affected by many factors, such as the excavation rate, the real-time excavation depth, changes in groundwater level, internal friction angle, soil weight, and number of supports [10–14]. Thus, the prediction of the foundation pit settlements and deformation is difficult and inaccurate [15]. Contributing to this situation are engineering accidents constantly occurring in many fields, such as building collapse, road or bridge cracks, excessive settlement of deep foundation pits, and pipeline bursts, accompanied by huge casualties and economic losses [16–22]. So, it is of great significance to accurately predict settlement values of foundation pits [23]. Compared to the settlement of the top of foundation pit, the settlement around the foundation pit is more complex and difficult to accurately predict, while traditional finite element methods, such as Midas, Plaxis, and Flac, have difficulty in achieving good results for the complexity of foundation pits [24–26]. With the rapid development of urbanization, more and more foundation pits are in the interior of the city, which means that the influence of the foundation pit settlement is increased, such as road cracking, uneven settlement of pile foundation of highway, and collapse of buildings.

Nowadays, lots of methods to forecast the foundation pit settlement have been established. In 2011, a new neural

network model was proposed by Ismail and Jeng, whose the features of SPT data along the excavation depth direction of the pile are set as the input samples to calculate the load-settlement curve for predicting the subsequent settlement [27]. Ghorbani and Niavol developed a new model to predict the settlement of the foundation pit under the circumstance of dynamic-static [28]. Lv et al. proposed a new model, which is based on grey theory and BP neural network to calculate the settlement around a foundation pit [29]. The results showed that two models have good application in engineering project, while the error of the models is still high and time factor is still the only input factor to be considered. Eid and Shehada proposed a method to the initial elastic settlement for the rock foundations [30]. Xu et al. presented the hybrid GA/SIMPLS to study the deformation law of the foundation pit [31]. Guo et al. conducted a new multivariable grey self-memory coupled prediction model, with high resolution prediction results of deep foundation pit [32]. Shahin established a model, which is based on the recurrent neural networks, to simulate the settlement response for bored piles under axial loading [33]. Doherty et al. studied an international project, which evaluated the responsiveness of geotechnical engineering, to analyze prediction of foundation settlement under the load of the undrained system [34]. Nejad and Jaksa established the ANN and CPT data to simulate the load settlement, while whole load-settlement relationship is obtained [35]. Cao et al. proposed a new neural network, which is an ensemble-based parameter sensitivity analysis paradigm, to study the impact of different parameters on the settlement. The result shows that the settlement is affected by many factors [36]. Su et al. put forward a settlement monitoring method on the basis of the Kalman filter, and the settlement is studied by forward modeling. The results show that it can predict the deformation of the following stage by analyzing the data of the prior stage [37]. Dai et al. filtered the observed that the noise and unmonitored data of the space and time domain are interpolated. The deformation of the dam was predicted through a Kalman filter recursive algorithm. The results demonstrate that the spatiotemporal noise of deformation can be effectively filtered out, and the deformation of the dam can be predicted well [38]. The wavelet packet transform and least-square support vector machines are combined, which are proposed by Zhang et al., to increase the accuracy and application in estimation of the ground subsidence under tunnel project [39]. Zhang et al. developed an optimized grey discrete Verhulst model-BP neural network to forecast the settlement of foundation pits [40].

Previous studies demonstrated that the relationship between the settlement and excavation time is characterized as an "S" curve, when the conditions are satisfied with linear loading [41, 42]. Meanwhile, the grey Verhulst model is commonly adopted to predict the settlement caused by the "S" characteristics [43–45]. In fact, the grey Verhulst model is more suitable for the prediction of the settlement of foundation pits where the amount of monitoring data is lacking and there are small settlement fluctuations in the short term [32, 40, 46]. It is mainly because the grey Verhulst model lacked the ability of self-learning and correcting the error [47, 48]. Nowadays, ANN has been used in various fields of engineering and plays an important role in predicting and distinguishing, while the BP neural network is one of the most widely used ANN in engineering fields for its strong ability of self-learning, information processing, nonlinear mapping, error feedback adjustment, and fault tolerance [49, 50]. Though the BP neural network has such advantages in predicting foundation pit settlements, it still has limitation in optimizing weights and thresholds, for easily falling into the local optimum [51, 52], while the genetic algorithm, which can be obtained by the near-optimal solutions in every search space, can well solve these problems [53, 54]. Therefore, a genetic algorithm (GA) is adopted to optimize the weights and thresholds of the BP neural network. On the contrary, the training process needs high-quantity and representative data [55]. In fact, it is hard to obtain accuracy and enough data in an actual engineering project, caused by the complicated influencing factors. Thus, the error will extremely lack an adequate training process. As for the grey Verhulst model, it can conduct a forecast for the data sequence in nonlinear and uncertain systems with insufficient data [32, 47, 56]. Therefore, the GA-BP neural network optimized by the grey Verhulst model is used to predict the settlement around foundation pits.

Meanwhile, in the preview study, the amount of training data is extremely insufficient, in which the amount of training data is often less than 20 sets, and the amount of prediction data is usually less than 10 sets [12, 40, 43, 57, 58]. It is mainly because the units of training data and prediction data are often set as month and week [40]. Not only that, time is often set as the only input parameter [12, 57, 58]. However, the settlement of the foundation pit is influenced by many factors, such as the internal friction angle, cohesion, bulk density, Poisson's ratio, void ratio, changes of real-time water level, permeability coefficient, the number of supports, and real-time excavation depth. Cause of the settlement of foundation pits is influenced by such many parameters; thus, it is inaccurate and meaningless to only study the influence of excavation time on the settlement of foundation pits. In addition, compared to the monthly or weekly accumulated settlement, the prediction of settlement that can be accurate to a certain day or a certain excavation depth has higher engineering significance. In this paper, the internal friction angle, cohesion, bulk density, Poisson's ratio of different soils, void ratio, changes of water level, permeability coefficient, number of supports, and real-time excavation depth are set as the input factors to predict the settlement around the foundation pits, which is nearby a pile foundation of a highway and larger settlement than other settlement monitoring points.

2. Methodology

The grey Verhulst model was proposed by Verhulst and Malthus to predict the procedure of featured saturation [59]. It is assumed that the $x^{(0)}(i)$ is the settlement value for the i-th monitoring, while the $x^{(1)}(i)$ is the accumulated generating operation of $x^{(0)}(i)$. The $x^{(0)}(i)$ and $x^{(1)}(i)$ are shown as follows:

$$X^{(0)} = \left\{x^{(0)}(1), x^{(0)}(2),\cdots,x^{(0)}(n)\right\}, \tag{1}$$

$$X^{(1)} = \left\{x^{(1)}(1), x^{(1)}(2),\cdots,x^{(1)}(n)\right\}, \tag{2}$$

where $x^{(1)}(k) = \sum_{i=1}^{k} x^{(0)}(k)$, $k = 1, 2, 3, \cdots, n$, while the $Z^{(1)} = \{z^{(1)}(1), z^{(1)}(2),\cdots,z^{(1)}(n)\}$ is the mean sequence of $x^{(1)}(k)$, where $z^{(1)}(k) = 1/2(x^{(1)}(k) + x^{(1)}(k-1))$, $k = 2, 3, \cdots, n$. The grey Verhulst model is shown as [60]

$$x^{(0)}(k) + az^{(1)}(k) = b\left(z^{(1)}(k)\right)^2, \tag{3}$$

where the $x^{(0)}(k)$ is named as the grey derivative; a and b are the development coefficient and grey factor, respectively; and the $z^{(1)}(k)$ is called the background value [61]. In particular, the parameters a and b are determined by the least-square method [62]. The parameter vectors of a and b are shown as

$$\widehat{a} = [a, b] = \left(B^T B\right)^{-1} B^T Y, \tag{4}$$

where

$$B = \begin{bmatrix} -z^{(1)}(2) & \left(z^{(1)}(2)\right)^2 \\ \vdots & \vdots \\ -z^{(1)}(n) & \left(z^{(1)}(n)\right)^2 \end{bmatrix}, \quad Y = \begin{bmatrix} x^{(0)}(2) \\ \vdots \\ x^{(0)}(n) \end{bmatrix}. \tag{5}$$

The whitenization differential Equation (6) of the grey Verhulst model, which is the first-order differential equation, can be obtained from the $x^{(1)}(k)$

$$\frac{dx^{(1)}}{dt} + ax^{(1)} = b\left(x^{(1)}\right)^2. \tag{6}$$

The resolution of the above Equation (6) is shown as

$$x\wedge^{(1)}(k+1) = \frac{1}{b/a + \left(1/x^{(1)}(1) - b/a\right)e^{ak}}, \tag{7}$$

where $k = 1, 2, 3, \cdots, n-1$.

As mentioned before, the grey Verhulst model lacks the ability to self-learn and correct the error. Due to the high ability of the BP neural network in information process self-learning, nonlinear mapping, and so on, BP neural networks are adopted in this paper.

While the BP neural network still has limitations in optimizing thresholds and weights, the GA is taken in this paper. The GA is adopted to acquire the near-optimal solutions.

Generally, the GA starts with an initial population using binary bits, such as 1 and 0, string generated through random ways. All the potential solutions, the integers, and the real numbers are encoded. The fitness is regarded as the key factor to evaluate the quality of each string in the problem's domain. Then, a better population will be created through genetic operators. And the BP neural network is optimized by the GA. The flow chart of the GA-BP neural network optimized by the grey Verhulst model is shown in Figure 1.

It can be seen in Figure 1 that the weight and thresholds of the BP neural network are encoded, when the topological structure is determined. The training process is determined by the thresholds and weights. In the genetic algorithm part (within the red rectangle), the crossover, fitness value, selection, and mutation are calculated. It decides if the new group is satisfactory; if not, the weights and thresholds are changed till the requirement is satisfied. As for the genetic algorithm (GA), the near-optimal solutions are obtained. Commonly, the GA commonly starts with the initial population using binary bits, such as 1 and 0, strings generated through random ways. All the integers, potential solutions, and real numbers are encoded by binary strings. And these are taken from search space, including with all the potential solutions. Then, strings are decoded into the search space, while the performance of these strings is evaluated by computing the fitness value for the objective function. In particular, the fitness is the key factor of the quality of each string in the problem's domain. After the strings are evaluated, a better population will be created through the genetic operators. In the end, the optimized weights and thresholds are obtained. While in the grey Verhulst model part, the grey Verhulst model is determined after the original measured value is inputted. Then, the predicted values are determined through performed simulation. Moving forward, the grey prediction values are selected. As per the analysis of the flow chart, the training processes are conducted and the settlements are predicted based on the input parameters.

Most of the previous studies focused on the influence of time factor on the settlement prediction. Not only that, the time factor is often simplified to the unit of week and month. Meanwhile, the prediction of settlement is often the unit of the week or month, which is lacking in engineering guiding significance. Since the settlement is the result of multiple factors, it is inaccurate and meaningless to consider excavation time only.

In this paper, many factors that affect settlement are taken into account to predict the settlement. In the excavation of foundation pits, the soil mechanical parameters have great influence on the settlement, having small settlement values under good geological conditions, while having huge settlement values under bad geological conditions [36]. Previous studies rarely consider this factor, mainly because it is difficult to determine the type of soil at a certain day of excavation. Meanwhile, it is impractical to record the depth of

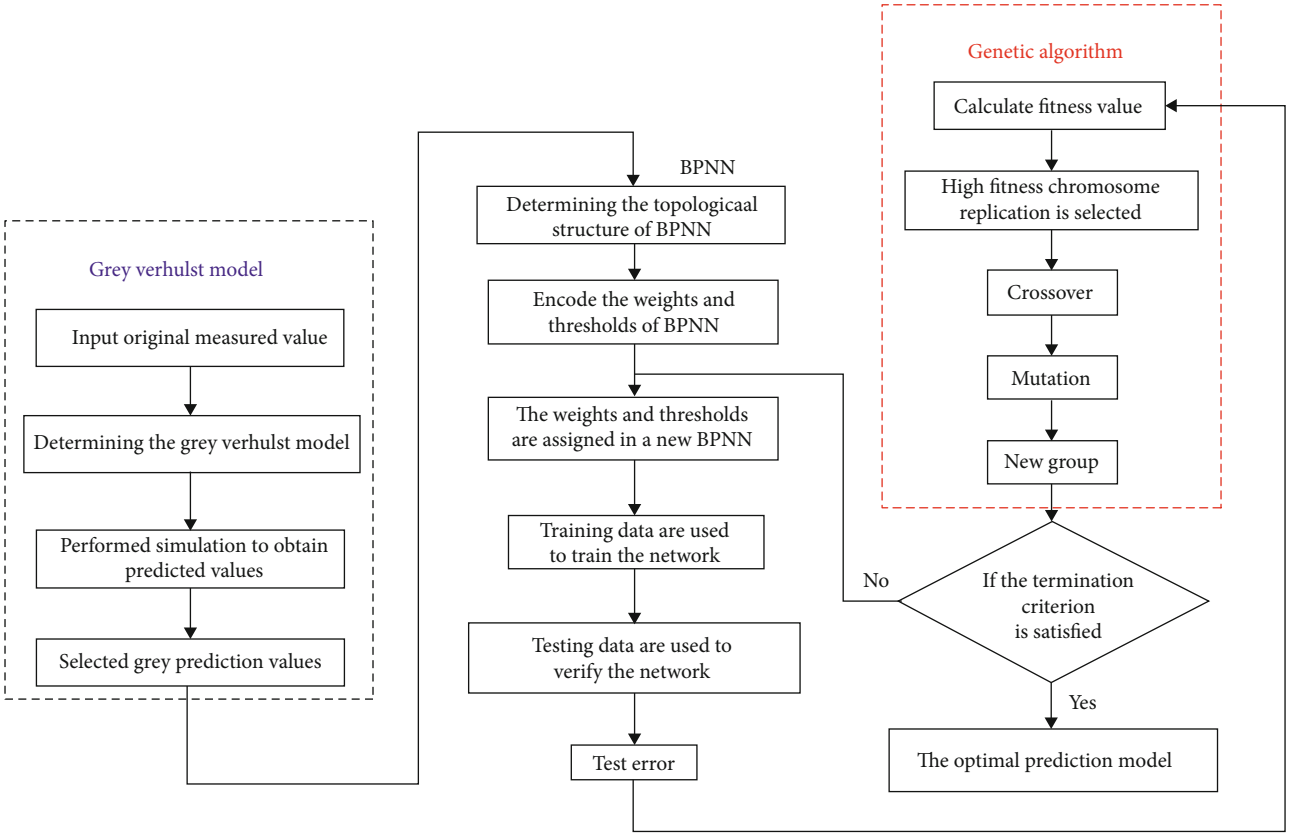

Figure 1: Flow chart of GA-BP neural network optimized by the grey Verhulst model.

excavation for each day, due to the complexity of excavation. To solve this issue, this paper proposed a method as follows. Firstly, supporting time and the position of different supports are precisely recorded. Then, the real-time excavation depth in the support position can be obtained, because these supports are set immediately when the foundation pit is excavated to the support position. After that, the excavation depth of the foundation pit is equally divided by the length of the excavation time between two adjacent support positions. Finally, the relationship between time and excavation depth can be established, which means the real-time excavation soil style can be confirmed, according to the drilling data. As for the internal support, the number of internal supports is increasing when the excavation depth is increasing, which can effectively decrease the deformation and settlement, while the number of the supports is adopted as the input parameters.

3. Application of Different Models in Settlement Prediction

The deep foundation pit project is located in Foshan City, Guangdong Province. This project consists of the receiving well, the jacking well, and the pipe jacking tunnel. Compared with the receiving well, the jacking well is taken as the research object due to its more complicated geological conditions, deeper excavation depth, and proximity to a bridge pier, to which the settlement around the foundation pit can induce adverse effects. In the process of foundation pit excavation, the settlement must be monitored during the whole excavation procedure. Different forms of monitoring points are set in Figure 2.

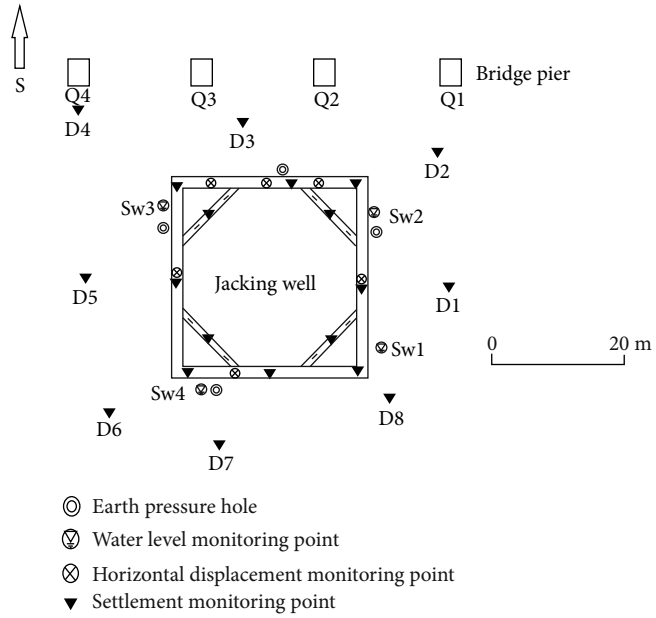

Figure 2: Different forms of monitoring points.

Table 1: The properties of rock-soil mass.

Category	Internal friction angle (°)	Cohesion (kPa)	Bulk density (kN·m^{-3})	Poisson's ratio	Void ratio	Permeability coefficient (m·d^{-1})
Plain fill	12	6	19	0.29	0.92	0.864
Muddy soil	6.2	9.66	17.2	0.3	1.2	5.27*E*-05
Silt	24	2	18	0.33	0.78	1.04
Medium sand	30	3	19.5	0.34	0.67	19.3
Calcareous siltstone	45	65	24.5	0.25	0.8	8.64*E*-6

The structure of the foundation pit and the distribution along the depth direction of soils are precisely matched as shown in Figure 3.

The settlement monitoring points around foundation pits are set as in Figure 2, which consist of D1-D8. Compared with other settlement monitoring points, the settlement of the D4 point (approximately 20 m southeast of the foundation pit) is the largest. Not only that, the D4 point is also close to the bridge pier of the highway. It means that the settlement of D4 may have a bad impact to the bridge pier, which is part of the highway. Therefore, the settlement of D4 is studied in this paper. Meanwhile, the project is located in Foshan city, Guangdong Province, where rainfall is heavy and concentrated. Thus, the water level around this foundation pit should also be considered. The SW1, SW2, SW3, and SW4 are water level monitoring points. In this paper, the water level changes are set as the input factor for training and prediction.

The characteristics and distribution of the rock-soil mass are obtained by geological data and drilling result. In particular, specimens of rock-soil mass are precisely obtained along different depths of drilling holes to obtain the rock-soil mass properties. Thus, the properties of the rock-soil mass are shown in Table 1.

The relationship between the real-time excavation time and the excavation soil type is demonstrated in detail above in this paper. Meanwhile, the water level changes are precisely match with the excavation time, while different permeability coefficients of the rock-soil mass are also considered in this paper to improve the accuracy of settlement prediction. The foundation pit project started on February 2, 2019, and the excavation to the bottom was on August 8, 2019 (188 days in total). The part monitoring data about the foundation pit settlement and related soil physical parameters are shown in Table 2 (for the detailed data, please refer to the supplemental files of Table 2).

As shown in Table 2, a day is 1 monitoring period, and settlement data sets of 188 days are selected, which is the whole process of foundation pit excavation. When the foundation pit was excavated to the depth of -10 meters (150th point) above sea level, the settlement of D4 was -31.52 mm. Up to 150 days, there was still 13 m deep of soil that needed to be excavated. In order to prevent the settlement of D4 from being too large, it is extremely important to predict the settlement of D4 continuing the existing construction conditions. Thus, the first 150 data sets are used to establish the model, and the last 38 data sets are taken to verify the accuracy of the trained model. In order to verify the accuracy and application of the GA-BP neural network optimized grey

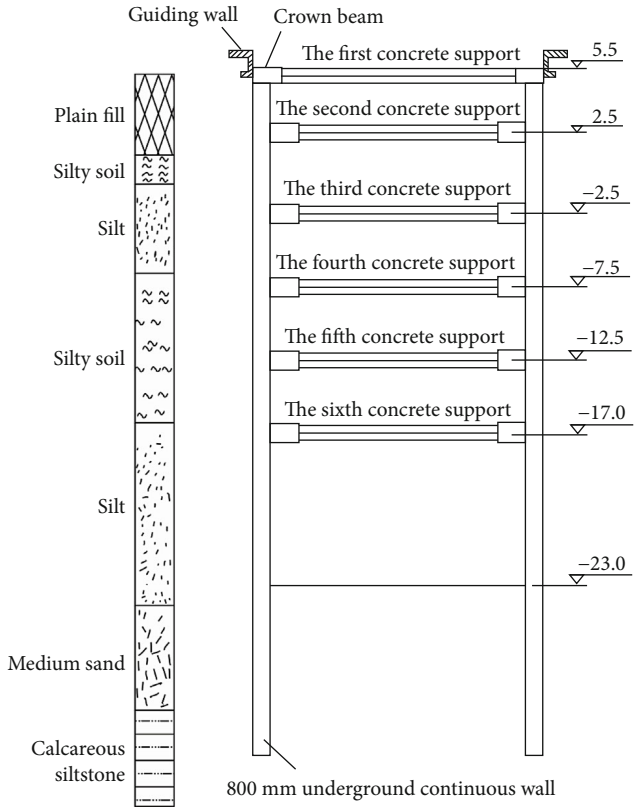

Figure 3: The structure of foundation pits and distribution along the depth direction of soils.

Verhulst model, four other models are compared, which consists of the grey Verhulst model, BP neural network, BP neural network optimized by grey Verhulst model, and BP neural network optimized by genetic algorithm (GA-BP neural network).

The grey Verhulst model is obtained through the first 150 actual settlement measured values (shown as the following equation):

$$x(k+1) = \frac{-17.3341}{1 - 0.4667 \times e^{0.0059}}. \tag{8}$$

Then, predicted results of the grey Verhulst model are inputted to the BP neural network, while the original data are set as the target value of the input vector to the BP neural

Table 2: Part monitoring data of the foundation pit settlement and related soil physical parameters.

Time/day	Internal friction angle/°	Cohesion/kPa	Bulk density/ ($kN \cdot m^{-3}$)	Poisson's ratio	Void ratio	SW3/m	SW2m	SW4/m	SW1/m	Permeability coefficient/($m \cdot d^{-1}$)	Num. of supports	Excavation depth/m	settlement/mm
1	12	6	19	0.29	0.92	-3.692	-3.697	-3.56	-4.092	0.864	1	5.5	0
2	12	6	19	0.29	0.92	-3.717	-3.697	-3.563	-4.145	0.864	1	5.3928571	0.85
3	12	6	19	0.29	0.92	-3.74	-3.734	-3.605	-4.15	0.864	1	5.2857143	-0.91
4	12	6	19	0.29	0.92	-3.758	-3.825	-3.617	-4.082	0.864	1	5.1785714	-0.43
5	12	6	19	0.29	0.92	-3.806	-3.855	-3.585	-4.04	0.864	1	5.0714286	-0.55
6	12	6	19	0.29	0.92	-3.573	-3.793	-3.592	-4.044	0.864	1	4.9642857	-1.01
7	12	6	19	0.29	0.92	-3.613	-3.78	-3.604	-4.034	0.864	1	4.8571429	-2.06
8	12	6	19	0.29	0.92	-3.815	-3.708	-3.566	-3.968	0.864	1	4.75	-2.68
9	12	6	19	0.29	0.92	-3.575	-3.686	-3.552	-3.907	0.864	1	4.6428571	-2.29
10	12	6	19	0.29	0.92	-3.58	-3.668	-3.544	-3.881	0.864	1	4.5357143	-1.95
11	12	6	19	0.29	0.92	-3.601	-3.774	-3.58	-3.889	0.864	1	4.4285714	-2.894
12	12	6	19	0.29	0.92	-3.613	-3.764	-3.59	-3.87	0.864	1	4.3214286	-3.219636
13	12	6	19	0.29	0.92	-3.852	-3.713	-3.578	-3.84	0.864	1	4.2142857	-3.545273
14	12	6	19	0.29	0.92	-3.608	-3.753	-3.562	-3.841	0.864	1	4.1071429	-3.870909
15	12	6	19	0.29	0.92	-3.603	-3.787	-3.595	-3.825	0.864	1	4	-4.196545
16	12	6	19	0.29	0.92	-3.621	-3.750	-3.575	-3.774	0.864	1	3.8928571	-4.522182
17	12	6	19	0.29	0.92	-3.614	-3.750	-3.574	-3.749	0.864	1	3.7857143	-4.847818
18	12	6	19	0.29	0.92	-3.607	-3.750	-3.574	-3.724	0.864	1	3.6785714	-5.173455
19	12	6	19	0.29	0.92	-3.600	-3.750	-3.573	-3.699	0.864	1	3.5714286	-5.499091
20	12	6	19	0.29	0.92	-3.593	-3.750	-3.572	-3.674	0.864	1	3.4642857	-5.824727
21	12	6	19	0.29	0.92	-3.587	-3.750	-3.573	-3.649	0.864	1	3.3571429	-6.150364
22	12	6	19	0.29	0.92	-3.580	-3.750	-3.571	-3.624	0.864	1	3.25	-6.476
23	12	6	19	0.29	0.92	-3.573	-3.751	-3.571	-3.599	0.864	1	3.1428571	-6.801636
24	12	6	19	0.29	0.92	-3.566	-3.755	-3.570	-3.574	0.864	1	3.0357143	-7.127273
25	12	6	19	0.29	0.92	-3.559	-3.751	-3.569	-3.549	0.864	1	2.9285714	-7.452909
26	12	6	19	0.29	0.92	-3.552	-3.752	-3.569	-3.524	0.864	1	2.8214286	-7.778545
27	12	6	19	0.29	0.92	-3.545	-3.751	-3.568	-3.500	0.864	1	2.7142857	-8.104182
28	12	6	19	0.29	0.92	-3.63	-3.784	-3.617	-3.837	0.864	1	2.6071429	-8.429818
29	12	6	19	0.29	0.92	-3.79	-3.794	-3.717	-3.845	0.864	2	2.5	-8.126667
30	12	6	19	0.29	0.92	-3.766	-3.79	-3.69	-3.82	0.864	2	2.3529412	-8.306667
31	12	6	19	0.29	0.92	-3.745	-3.781	-3.708	-3.834	0.864	2	2.2058824	-8.44
32	12	6	19	0.29	0.92	-3.8	-3.774	-3.7	-3.853	0.864	2	2.0588235	-8.76
33	12	6	19	0.29	0.92	-3.764	-3.793	-3.701	-3.835	0.864	2	1.9117647	-8.8
34	12	6	19	0.29	0.92	-3.697	-3.782	-3.675	-3.710	0.864	2	1.7647059	-8.913225
35	12	6	19	0.29	0.92	-3.757	-3.755	-3.682	-3.822	0.864	2	1.6176471	-9.38

Table 2: Continued.

Time/day	Internal friction angle/°	Cohesion/kPa	Bulk density/ ($kN \cdot m^{-3}$)	Poisson's ratio	Void ratio	SW3/m	SW2m	SW4/m	SW1/m	Permeability coefficient/($m \cdot d^{-1}$)	Num. of supports	Excavation depth/m	settlement/mm
36	12	6	19	0.29	0.92	-3.785	-3.787	-3.719	-3.837	0.864	2	1.4705882	-9.845679
37	12	6	19	0.29	0.92	-3.626	-3.627	-3.544	-3.696	0.864	2	1.3235294	-9.84
38	12	6	19	0.29	0.92	-3.598	-3.581	-3.493	-3.638	0.864	2	1.1764706	-10.45
39	12	6	19	0.29	0.92	-3.52	-3.47	-3.615	-3.59	0.864	2	1.0294118	-10.60468
40	6.2	9.66	17.2	0.3	1.2	-3.554	-3.525	-3.407	-3.568	5.27E-05	2	0.8823529	-10.89
41	6.2	9.66	17.2	0.3	1.2	-3.449	-3.467	-3.321	-3.532	5.27E-05	2	0.7352941	-11.08
42	6.2	9.66	17.2	0.3	1.2	-3.482	-3.409	-3.288	-3.475	5.27E-05	2	0.5882353	-11.97
43	6.2	9.66	17.2	0.3	1.2	-3.422	-3.386	-3.218	-3.451	5.27E-05	2	0.4411765	-11.18
44	6.2	9.66	17.2	0.3	1.2	-3.404	-3.378	-3.214	-3.439	5.27E-05	2	0.2941176	-11.41
45	6.2	9.66	17.2	0.3	1.2	-3.432	-3.184	-3.204	-3.459	5.27E-05	2	0.1470588	-11.58
46	6.2	9.66	17.2	0.3	1.2	-3.41	-3.402	-3.202	-3.502	5.27E-05	2	0	-11.52
47	6.2	9.66	17.2	0.3	1.2	-3.39	-3.32	-2.82	-3.483	5.27E-05	2	-0.147059	-11.83
48	6.2	9.66	17.2	0.3	1.2	-3.416	-3.343	-2.681	-3.422	5.27E-05	2	-0.294118	-12.18
49	6.2	9.66	17.2	0.3	1.2	-3.407	-3.398	-1.205	-3.465	5.27E-05	2	-0.441176	-11.96
50	24	2	18	0.33	0.78	-3.247	-3.345	-2.528	-3.39	1.04	2	-0.588235	-12.21
51	24	2	18	0.33	0.78	-2.528	-3.251	-1.689	-3.337	1.04	2	-0.735294	-12.42
52	24	2	18	0.33	0.78	-2.931	-3.224	-1.718	-3.255	1.04	2	-0.882353	-12.73
53	24	2	18	0.33	0.78	-2.933	-3.124	-1.848	-3.132	1.04	2	-1.029412	-13.59
54	24	2	18	0.33	0.78	-2.936	-2.997	-1.945	-3.043	1.04	2	-1.176471	-12.8
55	24	2	18	0.33	0.78	-2.924	-2.972	-2.026	-3.012	1.04	2	-1.323529	-13.58
56	24	2	18	0.33	0.78	-2.95	-2.988	-2.08	-3.04	1.04	2	-1.470588	-13.98
57	24	2	18	0.33	0.78	-3.025	-3.065	-2.17	-3.116	1.04	2	-1.617647	-13.98
58	24	2	18	0.33	0.78	-3.068	-3.125	-2.233	-3.174	1.04	2	-1.764706	-14.45
59	24	2	18	0.33	0.78	-3.141	-3.199	-2.292	-3.245	1.04	2	-1.911765	-14.8
60	24	2	18	0.33	0.78	-3.125	-3.192	-2.29	-3.235	1.04	2	-2.058824	-14.81
61	24	2	18	0.33	0.78	-3.184	-3.21	-2.331	-3.253	1.04	2	-2.205882	-14.88
62	24	2	18	0.33	0.78	-3.145	-3.185	-2.362	-3.232	1.04	2	-2.352941	-14.68
63	24	2	18	0.33	0.78	-3.143	-3.205	-2.43	-3.241	1.04	3	-2.5	-15.42
64	24	2	18	0.33	0.78	-3.201	-3.221	-2.505	-3.254	1.04	3	-2.563291	-15.65
65	24	2	18	0.33	0.78	-3.135	-3.218	-2.521	-3.252	1.04	3	-2.626582	-15.85
66	24	2	18	0.33	0.78	-3.176	-3.258	-2.575	-3.283	1.04	3	-2.689873	-16.64
67	24	2	18	0.33	0.78	-3.446	-3.347	-2.693	-3.377	1.04	3	-2.753165	-17.75
68	24	2	18	0.33	0.78	-3.253	-3.344	-2.708	-3.358	1.04	3	-2.816456	-17.92
69	24	2	18	0.33	0.78	-3.21	-3.275	-2.665	-3.278	1.04	3	-2.879747	-17.81
70	24	2	18	0.33	0.78	-3.223	-3.297	-2.734	-3.3	1.04	3	-2.943038	-16.99

Table 2: Continued.

Time/day	Internal friction angle/°	Cohesion/kPa	Bulk density/ ($kN \cdot m^{-3}$)	Poisson's ratio	Void ratio	SW3/m	SW2m	SW4/m	SW1/m	Permeability coefficient/($m \cdot d^{-1}$)	Num. of supports	Excavation depth/m	settlement/mm
71	24	2	18	0.33	0.78	-3.244	-3.279	-2.748	-3.292	1.04	3	-3.006329	-17.22
72	24	2	18	0.33	0.78	-3.224	-3.192	-2.688	-3.284	1.04	3	-3.06962	-16.94
73	24	2	18	0.33	0.78	-3.229	-3.324	-2.798	-3.343	1.04	3	-3.132911	-18.29
74	24	2	18	0.33	0.78	-3.272	-3.328	-2.79	-3.381	1.04	3	-3.196203	-19.54
75	24	2	18	0.33	0.78	-3.239	-3.334	-2.669	-3.355	1.04	3	-3.259494	-19.14
76	24	2	18	0.33	0.78	-3.287	-3.268	-2.723	-3.262	1.04	3	-3.322785	-20.49
77	24	2	18	0.33	0.78	-3.185	-3.258	-2.758	-3.242	1.04	3	-3.386076	-20.39
78	24	2	18	0.33	0.78	-3.23	-3.296	-2.81	-3.25	1.04	3	-3.449367	-19.16
79	24	2	18	0.33	0.78	-3.195	-3.258	-2.833	-3.222	1.04	3	-3.512658	-19.78
80	24	2	18	0.33	0.78	-3.188	-3.232	-2.865	-3.22	1.04	3	-3.575949	-20.52
81	24	2	18	0.33	0.78	-3.237	-3.263	-2.894	-3.222	1.04	3	-3.639241	-20.52
82	24	2	18	0.33	0.78	-3.185	-3.263	-2.915	-3.233	1.04	3	-3.702532	-19.2
83	24	2	18	0.33	0.78	-3.214	-3.288	-2.952	-3.263	1.04	3	-3.765823	-18.73
84	24	2	18	0.33	0.78	-3.16	-3.336	-2.962	-3.248	1.04	3	-3.829114	-20.28
85	24	2	18	0.33	0.78	-3.215	-3.252	-2.973	-3.288	1.04	3	-3.892405	-21.01
86	24	2	18	0.33	0.78	-3.2	-3.275	-2.966	-3.284	1.04	3	-3.955696	-22.01
87	24	2	18	0.33	0.78	-3.433	-3.264	-2.887	-3.253	1.04	3	-4.018987	-22.17
88	24	2	18	0.33	0.78	-3.122	-3.223	-2.447	-3.178	1.04	3	-4.082278	-22.31
89	24	2	18	0.33	0.78	-3.082	-3.02	-2.377	-3.088	1.04	3	-4.14557	-21.92
90	24	2	18	0.33	0.78	-2.992	-3.055	-2.336	-3.1	1.04	3	-4.208861	-23.36
91	24	2	18	0.33	0.78	-2.92	-2.98	-2.33	-3.01	1.04	3	-4.272152	-22.69
92	24	2	18	0.33	0.78	-2.917	-2.928	-2.324	-2.902	1.04	3	-4.335443	-23.4
93	24	2	18	0.33	0.78	-2.92	-2.912	-2.341	-2.89	1.04	3	-4.398734	-22.55
94	24	2	18	0.33	0.78	-2.771	-2.778	-2.297	-2.748	1.04	3	-4.462025	-23.65
95	24	2	18	0.33	0.78	-3.043	-2.736	-2.231	-2.669	1.04	3	-4.525316	-23.08
96	24	2	18	0.33	0.78	-2.813	-2.712	-2.219	-2.629	1.04	3	-4.588608	-23.34
97	24	2	18	0.33	0.78	-2.853	-2.775	-2.267	-2.685	1.04	3	-4.651899	-22.56
98	24	2	18	0.33	0.78	-2.852	-2.788	-1.846	-2.718	1.04	3	-4.71519	-23.17
99	24	2	18	0.33	0.78	-2.877	-2.828	-2.026	-2.738	1.04	3	-4.778481	-23.48
100	24	2	18	0.33	0.78	-2.91	-2.888	-2.17	-2.793	1.04	3	-4.841772	-24.16
101	24	2	18	0.33	0.78	-2.894	-2.923	-2.188	-2.824	1.04	3	-4.905063	-25.78
102	24	2	18	0.33	0.78	-2.896	-2.887	-2.224	-2.764	1.04	3	-4.968354	-24.41
103	24	2	18	0.33	0.78	-2.833	-2.834	-2.167	-2.678	1.04	3	-5.031646	-23.68
104	24	2	18	0.33	0.78	-2.938	-2.788	-2.112	-2.637	1.04	3	-5.094937	-26.52
105	24	2	18	0.33	0.78	-2.861	-2.848	-2.197	-2.698	1.04	3	-5.158228	-24.87

Table 2: Continued.

Time/day	Internal friction angle/°	Cohesion/kPa	Bulk density/ ($kN \cdot m^{-3}$)	Poisson's ratio	Void ratio	SW3/m	SW2m	SW4/m	SW1/m	Permeability coefficient/($m \cdot d^{-1}$)	Num. of supports	Excavation depth/m	settlement/mm
106	24	2	18	0.33	0.78	-2.832	-2.873	-2.27	-2.728	1.04	3	-5.221519	-26.49
107	24	2	18	0.33	0.78	-2.845	-2.856	-2.299	-2.723	1.04	3	-5.28481	-26.01
108	24	2	18	0.33	0.78	-2.832	-2.848	-2.149	-2.682	1.04	3	-5.348101	-25.61
109	24	2	18	0.33	0.78	-2.804	-2.795	-2.11	-2.657	1.04	3	-5.411392	-25.48
110	24	2	18	0.33	0.78	-2.727	-2.713	-2.084	-2.588	1.04	3	-5.474684	-25.2
111	24	2	18	0.33	0.78	-2.668	-2.638	-2.051	-2.503	1.04	3	-5.537975	-25.84
112	24	2	18	0.33	0.78	-2.71	-2.67	-2.06	-2.508	1.04	3	-5.601266	-26.62
113	24	2	18	0.33	0.78	-2.917	-2.716	-2.135	-2.533	1.04	3	-5.664557	-26.22
114	24	2	18	0.33	0.78	-2.815	-2.778	-2.202	-2.595	1.04	3	-5.727848	-27.99
115	24	2	18	0.33	0.78	-2.842	-2.822	-2.245	-2.649	1.04	3	-5.791139	-26.99
116	24	2	18	0.33	0.78	-2.862	-2.871	-2.308	-2.718	1.04	3	-5.85443	-27.71
117	24	2	18	0.33	0.78	-2.862	-2.871	-2.398	-2.718	1.04	3	-5.917722	-27.19
118	24	2	18	0.33	0.78	-2.827	-2.938	-2.451	-2.759	1.04	3	-5.981013	-27.02
119	24	2	18	0.33	0.78	-3.188	-2.934	-2.461	-2.754	1.04	3	-6.044304	-28.23
120	24	2	18	0.33	0.78	-2.95	-2.978	-2.501	-2.788	1.04	3	-6.107595	-27.65
121	24	2	18	0.33	0.78	-2.857	-3.037	-2.508	-2.805	1.04	3	-6.170886	-29.05
122	24	2	18	0.33	0.78	-2.868	-3.042	-2.585	-2.834	1.04	3	-6.234177	-30.39
123	24	2	18	0.33	0.78	-2.905	-3.061	-2.643	-2.855	1.04	3	-6.297468	-30.39
124	24	2	18	0.33	0.78	-2.923	-3.093	-2.688	-2.886	1.04	3	-6.360759	-29.92
125	24	2	18	0.33	0.78	-3.085	-3.069	-2.695	-2.869	1.04	3	-6.424051	-29.87
126	24	2	18	0.33	0.78	-2.974	-3.084	-2.695	-2.894	1.04	3	-6.487342	-29.51
127	24	2	18	0.33	0.78	-2.872	-3.111	-2.746	-2.932	1.04	3	-6.550633	-30.18
128	6.2	9.66	17.2	0.3	1.2	-2.798	-3.069	-2.505	-2.879	5.27E-05	3	-6.613924	-30.25
129	6.2	9.66	17.2	0.3	1.2	-2.754	-3.051	-2.23	-2.867	5.27E-05	3	-6.677215	-30.1
130	6.2	9.66	17.2	0.3	1.2	-2.781	-3.069	-2.296	-2.884	5.27E-05	3	-6.740506	-29.5
131	6.2	9.66	17.2	0.3	1.2	-2.836	-3.086	-2.409	-2.895	5.27E-05	3	-6.803797	-29.5
132	6.2	9.66	17.2	0.3	1.2	-2.671	-3.033	-2.116	-2.765	5.27E-05	3	-6.867089	-30.27
133	6.2	9.66	17.2	0.3	1.2	-2.71	-2.904	-2.181	-2.693	5.27E-05	3	-6.93038	-29.56
134	6.2	9.66	17.2	0.3	1.2	-2.627	-2.871	-2.179	-2.642	5.27E-05	3	-6.993671	-28.68
135	6.2	9.66	17.2	0.3	1.2	-2.492	-2.789	-2.022	-2.554	5.27E-05	3	-7.056962	-29.64
136	6.2	9.66	17.2	0.3	1.2	-2.53	-2.833	-1.942	-2.59	5.27E-05	3	-7.120253	-29.54
137	6.2	9.66	17.2	0.3	1.2	-2.484	-2.772	-2.054	-2.555	5.27E-05	3	-7.183544	-29.46
138	6.2	9.66	17.2	0.3	1.2	-2.575	-2.797	-2.068	-2.577	5.27E-05	3	-7.246835	-29.46
139	6.2	9.66	17.2	0.3	1.2	-2.567	-2.815	-2.077	-2.576	5.27E-05	3	-7.310127	-31.06
140	6.2	9.66	17.2	0.3	1.2	-2.58	-2.824	-2.165	-2.606	5.27E-05	3	-7.373418	-31.35

Table 2: Continued.

Time/day	Internal friction angle/°	Cohesion/kPa	Bulk density/ ($kN \cdot m^{-3}$)	Poisson's ratio	Void ratio	SW3/m	SW2m	SW4/m	SW1/m	Permeability coefficient/($m \cdot d^{-1}$)	Num. of supports	Excavation depth/m	settlement/mm
141	6.2	9.66	17.2	0.3	1.2	-2.604	-2.833	-2.244	-2.633	5.27E-05	3	-7.436709	-31.35
142	6.2	9.66	17.2	0.3	1.2	-2.621	-2.849	-2.292	-2.625	5.27E-05	4	-7.5	-31.35
143	6.2	9.66	17.2	0.3	1.2	-3.029	-2.85	-2.325	-2.617	5.27E-05	4	-7.857143	-31.35
144	6.2	9.66	17.2	0.3	1.2	-2.618	-2.83	-2.221	-2.59	5.27E-05	4	-8.214286	-31.35
145	6.2	9.66	17.2	0.3	1.2	-2.559	-2.784	-2.074	-2.516	5.27E-05	4	-8.571429	-31.35
146	6.2	9.66	17.2	0.3	1.2	-2.427	-2.624	-1.949	-2.386	5.27E-05	4	-8.928571	-31.35
147	6.2	9.66	17.2	0.3	1.2	-2.347	-2.539	-1.896	-2.27	5.27E-05	4	-9.285714	-33.52
148	6.2	9.66	17.2	0.3	1.2	-2.334	-2.457	-1.901	-2.242	5.27E-05	4	-9.642857	-31.52
149	6.2	9.66	17.2	0.3	1.2	-2.41	-2.449	-1.915	-2.19	5.27E-05	4	-10	-31.31
150	6.2	9.66	17.2	0.3	1.2	-2.435	-2.532	-2.038	-2.279	5.27E-05	4	-10.35714	-32.11
151	6.2	9.66	17.2	0.3	1.2	-2.461	-2.628	-2.085	-2.346	5.27E-05	4	-10.71429	-32.58
152	6.2	9.66	17.2	0.3	1.2	-2.198	-2.677	-1.978	-2.4	5.27E-05	4	-11.07143	-31.49
153	6.2	9.66	17.2	0.3	1.2	-2.57	-2.722	-2.021	-2.449	5.27E-05	4	-11.42857	-30.98
154	6.2	9.66	17.2	0.3	1.2	-2.576	-2.728	-2.167	-2.456	5.27E-05	4	-11.78571	-32.13
155	6.2	9.66	17.2	0.3	1.2	-2.688	-2.764	-2.282	-2.477	5.27E-05	4	-12.14286	-33.2
156	6.2	9.66	17.2	0.3	1.2	-2.742	-2.814	-2.362	-2.514	5.27E-05	5	-12.5	-33.2
157	6.2	9.66	17.2	0.3	1.2	-2.016	-2.854	-2.424	-2.562	5.27E-05	5	-12.71429	-34.8
158	6.2	9.66	17.2	0.3	1.2	-2.407	-2.753	-2.143	-2.457	5.27E-05	5	-12.92857	-34.8
159	6.2	9.66	17.2	0.3	1.2	-2.302	-2.724	-2.194	-2.422	5.27E-05	5	-13.14286	-34.74
160	6.2	9.66	17.2	0.3	1.2	-2.477	-2.68	-2.163	-2.398	5.27E-05	5	-13.35714	-33.06
161	6.2	9.66	17.2	0.3	1.2	-2.437	-2.713	-2.207	-2.434	5.27E-05	5	-13.57143	-34.15
162	6.2	9.66	17.2	0.3	1.2	-2.762	-2.743	-2.271	-2.454	5.27E-05	5	-13.78571	-34.57
163	6.2	9.66	17.2	0.3	1.2	-2.723	-2.763	-2.124	-2.482	5.27E-05	5	-14	-34.37
164	6.2	9.66	17.2	0.3	1.2	-2.607	-2.809	-2.272	-2.496	5.27E-05	5	-14.21429	-34.33
165	6.2	9.66	17.2	0.3	1.2	-2.771	-2.871	-2.262	-2.526	5.27E-05	5	-14.42857	-33.68
166	6.2	9.66	17.2	0.3	1.2	-2.493	-2.778	-2.137	-2.47	5.27E-05	5	-14.64286	-34.65
167	6.2	9.66	17.2	0.3	1.2	-2.512	-2.74	-2.084	-2.541	5.27E-05	5	-14.85714	-35.62
168	6.2	9.66	17.2	0.3	1.2	-3.163	-2.742	-2.154	-6.692	5.27E-05	5	-15.07143	-36.95
169	6.2	9.66	17.2	0.3	1.2	-2.962	-2.804	-2.345	-3.86	5.27E-05	5	-15.28571	-36.93
170	6.2	9.66	17.2	0.3	1.2	-3.33	-2.845	-2.424	-4.934	5.27E-05	5	-15.5	-37.14
171	6.2	9.66	17.2	0.3	1.2	-3.326	-2.848	-2.428	-4.928	5.27E-05	5	-15.71429	-37.19
172	6.2	9.66	17.2	0.3	1.2	-3.15	-2.842	-2.428	-4.645	5.27E-05	5	-15.92857	-37.5
173	24	2	18	0.33	0.78	-3.092	-2.843	-2.422	-4.055	1.04	5	-16.14286	-37.86
174	24	2	18	0.33	0.78	-2.495	-2.742	-2.082	-3.543	1.04	5	-16.35714	-37.8
175	24	2	18	0.33	0.78	-2.57	-2.68	-2.071	-2.84	1.04	5	-16.57143	-37.42

Table 2: Continued.

Time/day	Internal friction angle/°	Cohesion/kPa	Bulk density/ ($kN \cdot m^{-3}$)	Poisson's ratio	Void ratio	SW3/m	SW2m	SW4/m	SW1/m	Permeability coefficient/($m \cdot d^{-1}$)	Num. of supports	Excavation depth/m	settlement/mm
176	24	2	18	0.33	0.78	-2.502	-2.597	-2.092	-2.742	1.04	5	-16.78571	-37.42
177	24	2	18	0.33	0.78	-2.487	-2.59	-2.105	-2.732	1.04	6	-17	-37.42
178	24	2	18	0.33	0.78	-2.498	-2.645	-2.143	-2.717	1.04	6	-17.54545	-37.83
179	24	2	18	0.33	0.78	-2.49	-2.654	-2.132	-2.666	1.04	6	-18.09091	-38.39
180	24	2	18	0.33	0.78	-2.464	-2.631	-2.099	-2.662	1.04	6	-18.63636	-38.88
181	24	2	18	0.33	0.78	-2.423	-2.586	-2.036	-2.648	1.04	6	-19.18182	-39.3
182	24	2	18	0.33	0.78	-2.445	-2.632	-2.034	-2.693	1.04	6	-19.72727	-38.57
183	24	2	18	0.33	0.78	-2.458	-2.601	-2.023	-2.718	1.04	6	-20.27273	-39.86
184	24	2	18	0.33	0.78	-2.399	-2.736	-2.062	-2.783	1.04	6	-20.81818	-39.84
185	24	2	18	0.33	0.78	-1.919	-2.77	-2.055	-3.048	1.04	6	-21.36364	-40.27
186	24	2	18	0.33	0.78	-2.739	-2.964	-2.246	-3.058	1.04	6	-21.90909	-40.3
187	24	2	18	0.33	0.78	-2.394	-2.962	-2.318	-3.118	1.04	6	-22.45455	-40.49
188	24	2	18	0.33	0.78	-2.807	-3.02	-2.401	-3.014	1.04	6	-23	-41.57

network. Then, the weights and thresholds are optimized by the genetic algorithm. The training max epochs are 50000; the learning rate is $3e^{-3}$. The target error of the training is set as $1E$-10, while the highest failure time is selected as 6. The gradient descent method is used in this study. In MATLAB, the input layer uses the function "tansig," the hidden layer uses the function "logsig," and the "purelin" are selected in the output layer, while the best hidden neurons are 6, which is obtained after the training and testing processes. As for the best neurons of the GA-BP neural network and BP neural network, the best hidden neurons are both 6. The other parameters are same as the GA-BP neural network for the purpose of comparison. The comparison between measured values and different models, which consist of the BP neural network, the GA-BP neural network, the BP neural network optimized by grey Verhulst model, and the GA-BP neural network optimized by grey Verhulst model, is shown in Figure 4.

As shown in Figure 4, the predicted values of the BP neural network are compared with the measured values. It shows that the accuracy of the predicted values and the consistently measured values is relatively low. In particular, since day 167, the error between measured values and the predicted value has largely increased. The fluctuation of settlement values with time cannot be reflected well by the BP neural network, while the consistency between measured values and predicted values can be basically accepted before day 167, and the consistency is low after day 167. At day 188, the error between measured values and the predicted value is 3.502, while the relative error at day 188 is 8.42%. The changes of error show an increasing trend with the increase of time. And it is basically fitted with the feature of the prediction result, in which the prediction resolution decreased with the increase of the predicted data sets.

Due to the "S" characteristics of foundation pit settlements, the grey Verhulst model is often adopted to predict settlement due to its own characteristics. Then, the BP neural network is optimized by the grey Verhulst model to forecast the settlement. The comparison between predicted values and measured values of the BP neural network optimized by the grey Verhulst model is shown in Figure 5.

As shown in Figure 5, it can be easily found that the consistency is relatively high. It is mainly because the prediction process is optimized by the grey Verhulst model, which is very suitable for the prediction of the settlement. The blue oval (Figure 5) marks the peaks of the predicted polyline and the measured polyline with high consistency and resolution, while the green rectangle (Figure 5) marks the part polylines that also show a high consistency. Although the consistency between predicted values and measured values is high, it is worth noting that the error between measured values and predicted values, which is before day 170, is too large. It is mainly because the BP neural network easily falls into a local optimum, which is limited in optimizing weights and thresholds. As for the predicted values after day 170, the resolution of predicted results highly contributes to the correction of the grey Verhulst model. Due to the lack of predicted value accuracy

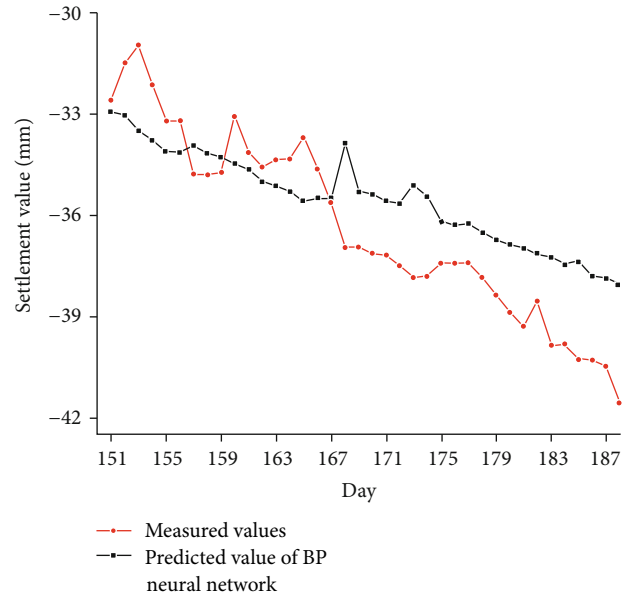

Figure 4: Comparison between measured values and predicted values of BP neural network.

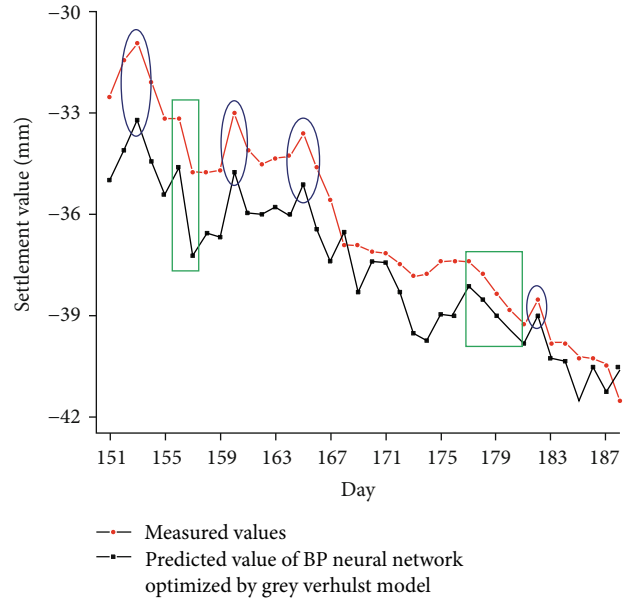

Figure 5: The comparison between measured values and predicted values of the BP neural network optimized by the grey Verhulst model.

before day 170, the BP neural network is optimized by the GA, which has the ability to optimize the weights and thresholds. The comparison between measured values and the predicted value of the GA-BP neural network are shown in Figure 6.

As shown in Figure 6, it can be obtained that the predicted values of the GA-BP neural network have high accuracy, in which the polyline of predicted values is almost in the internal position of the polyline of the measured values.

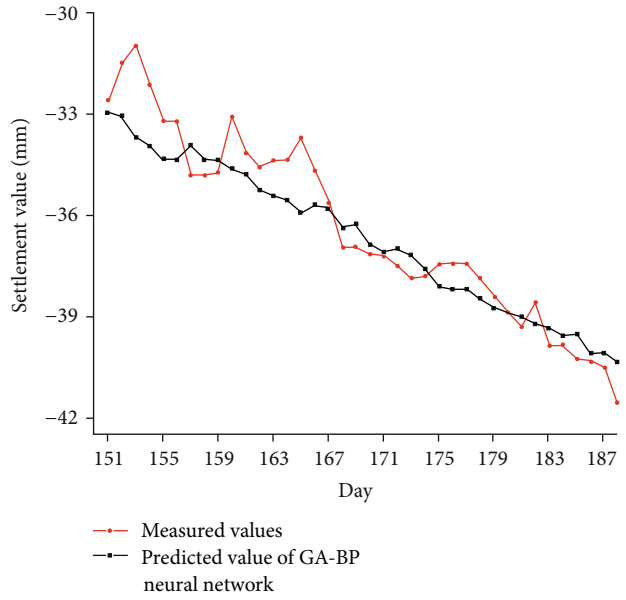

Figure 6: The comparison between measured values and predicted value of GA-BP neural network.

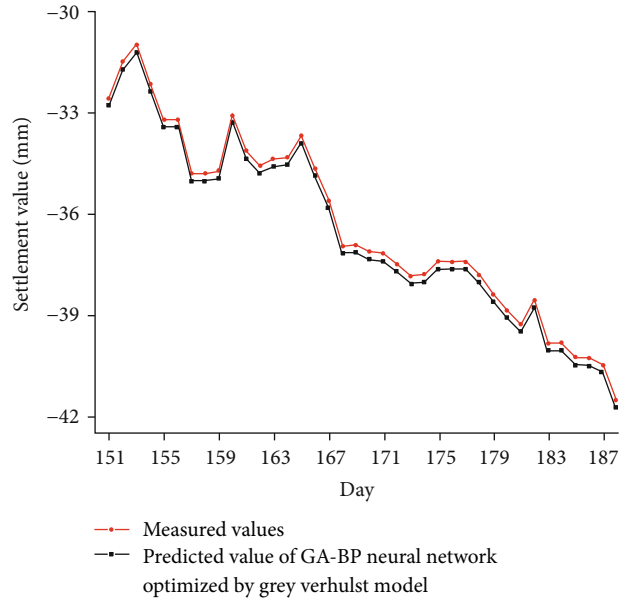

Figure 7: Comparison between measured values and predicted values of GA-BP neural network optimized by grey Verhulst model.

Comparing the Figures 4 and 6, it can be easily found that the prediction accuracy of the GA-BP neural network has largely improved compared to the prediction of the BP neural network, while compared to the BP neural network optimized by the grey Verhulst model, it is worth noting that the GA-BP neural network has low reflection to the fluctuation of the measured values. This conclusion also proved that the grey Verhulst model has good application to predict the settlement around the foundation pits on the other side. Through the above analysis, the GA-BP neural network optimized by the grey Verhulst model is used to predict the settlement of foundation pits, which has taken the advantage of the genetic algorithm and the grey Verhulst model. The comparison between measured values and predicted values of the GA-BP neural network optimized by the grey Verhulst model are shown in Figure 7.

As shown in Figure 7, the predicted values of the GA-BP neural network optimized by the grey Verhulst model have shown extremely high resolution and accuracy with the measured values. The polyline of predicted values almost coincides with the polyline of the measured values, which means extremely high consistency between predicted values and measured values. Comparing Figures 5 and 7, it can be seen that the accuracy of predicted values of the BP neural network optimized by the grey Verhulst model is greatly improved by the genetic algorithm, which means the genetic algorithm has good application in optimizing the BP neural network, which has been already optimized by the grey Verhulst model. Similarly, the reflection to the fluctuation of the GA-BP neural network is greatly improved through the optimization by the grey Verhulst model. In general, the GA-BP neural network optimized by the grey Verhulst model has high application and accuracy in the prediction of the settlement.

Usually, mean absolute error (MAE), coefficient of correlation (R^2), mean absolute percentage error (MAPE), mean square error (MSE), and root mean square error (RMSE) are used to evaluate the prediction resolution. The model is considered as excellent, when the errors in terms of MAPE, MAE, RMSE, and MSE are close to 0 and the R^2 is close to 1. In this paper, these evaluated parameters are used to further compare the predicted values of the BP neural network, BP neural network optimized by grey Verhulst model, GA-BP neural network, and GA-BP neural network optimized by grey Verhulst model with measured values. The comparison of these models is shown in Table 3.

As listed in Table 3, it can be obtained that the R^2 of the GA-BP neural network optimized by the grey Verhulst model is the closest to 1, while the RMSE, MSE, MAE, and MAPE are all the lowest compared with three other models. It means that the GA-BP neural network is superior to the three models in the prediction of settlement. In particular, though the consistency has greatly increased from the BP neural network to the BP neural network optimized by the grey Verhulst model, these evaluated parameters of the BP neural network optimized by the grey Verhulst are not greatly improved compared with the BP neural network, such as the RMSE has improved from 1.801 to 1.523, while compared to the GA-BP neural network and the BP neural network, the MSE has decreased from 3.245 to 0.942. In particular, the MAPE has decreased from 6.67% to 2.02%. But the analysis above demonstrates that the GA-BP neural network has low reflection to the fluctuation. So, the GA-BP neural network optimized by the grey Verhulst model, which has taken the two advantages of GA and the grey Verhulst model, should have higher resolution than the three other models in theory. The predicted result has well proven this assumption.

Table 3: Calculation results of performance indexes for these models.

Models	RMSE (mm)	MSE (mm^2)	MAE (mm)	MAPE (%)	R^2
BP neural network	1.801	3.245	1.592	6.67	0.570
BP neural network optimized by grey Verhulst model	1.523	2.319	1.348	8.84	0.692
GA-BP neural network	0.971	0.942	0.780	2.02	0.720
GA-BP neural network optimized by grey Verhulst model	0.221	0.049	0.221	1.59	0.994

4. Summary and Conclusions

Because of the influence of many factors, settlement around the foundation pit is hard to predict. In this paper, the settlement of D4 is studied due to a large settlement value and being close to the bridge pier of a highway. The internal friction angle, cohesion, bulk density, Poisson's ratio, void ratio, water level changes, permeability coefficient, number of supports, and excavation depth, which influence the settlement around foundation pits, are adopted as the input parameters of the prediction model. Since the supporting time is precisely recorded, the correspondence between the real-time excavation depth and the excavation time can be obtained. Then, the first 150 data sets are used to establish the model, and the last 38 data sets are taken to verify the accuracy of the established model. To obtain a suitable model, the BP neural network, GA-BP neural network, BP neural network optimized by grey Verhulst model, and GA-BP neural network optimized by grey Verhulst model are used to predict the settlement of foundation pits, and the comparisons are detailed analysed. The following conclusions can be advanced from this paper:

(1) Due to insufficient consideration of influencing factors in previous studies, the internal friction angle, cohesion, bulk density, Poisson's ratio, void ratio, water level changes, permeability coefficient, number of supports, and excavation depth are taken into consideration in this study. Through the analysis of the prediction results, the selection of these input parameters has high guiding significance for the prediction settlement around foundation pits

(2) This paper proposed a new model, which is combined with the BP neural, genetic algorithm, and grey Verhulst models, to predict the settlement of a certain day or excavation to a certain depth in a long period of time in the future, which has guiding significance for engineering construction

(3) The predicted values of the BP neural network, BP neural network optimized by the grey Verhulst model, GA-BP neural network, and GA-BP neural network optimized by the grey Verhulst model are compared with measured values. The results show that the grey Verhulst model can greatly improve the consistency between predicted values and measured values, while the accuracy of the early stage is low. It is mainly because the BP neural network easily falls into a local optimum. The genetic algorithm (GA), which can largely improve the accuracy of predicted values, has low reflection to the fluctuation of measured values. The GA-BP neural network optimized by the grey Verhulst model, which takes the advantages of the genetic algorithm (GA) and grey Verhulst model, has extremely high consistency and accuracy with measured values. The results of RMSE, MAE, R^2, and MSE further prove the conclusion

Data Availability

The experimental data used to support the findings of this study are included within the article.

Conflicts of Interest

The authors declare that there are no conflicts of interest regarding the publication of this paper.

References

[1] Y. He, B. B. Li, K. N. Zhang, Z. Li, Y. G. Chen, and W. M. Ye, "Experimental and numerical study on heavy metal contaminant migration and retention behavior of engineered barrier in tailings pond," *Environmental Pollution*, vol. 252, Part B, pp. 1010–1018, 2019.

[2] C. M. Zhang, "Applications of soil nailed wall in foundation pit support," *Applied Mechanics and Materials*, vol. 353-356, pp. 969–973, 2013.

[3] X. Zhang, Y. Wu, E. Zhai, and P. Ye, "Coupling analysis of the heat-water dynamics and frozen depth in a seasonally frozen zone," *Journal of Hydrology*, vol. 593, article 125603, 2020.

[4] J. Du, G. Zheng, B. Liu, N. J. Jiang, and J. Hu, "Triaxial behavior of cement-stabilized organic matter–disseminated sand," *Acta Geotechnica*, vol. 16, no. 1, pp. 211–220, 2021.

[5] C. Zhu, X. Xu, W. Liu, F. Xiong, and X. Liu, "Softening damage analysis of gypsum rock with water immersion time based on laboratory experiment," *IEEE Access*, vol. 7, pp. 125575–125585, 2019.

[6] C. Liu, Y. Wang, X. Zhang, and L. Du, "Rock brittleness evaluation method based on the complete stress-strain curve," *Frattura ed Integrità Strutturale*, vol. 13, no. 49, pp. 557–567, 2019.

[7] C. Liu, X. Hu, R. Yao et al., "Assessment of soil thermal conductivity based on BPNN optimized by genetic algorithm," *Advances in Civil Engineering*, vol. 2020, Article ID 6631666, 10 pages, 2020.

[8] W. Wang, L.-q. Li, W.-y. Xu, Q.-x. Meng, and J. Lu, "Creep failure mode and criterion of Xiangjiaba sandstone," *Journal of Central South University*, vol. 19, no. 12, pp. 3572–3581, 2012.

[9] L. L. Yang, W. Y. Xu, Q. X. Meng, and R. B. Wang, "Investigation on jointed rock strength based on fractal theory," *Journal of Central South University*, vol. 24, no. 7, pp. 1619–1626, 2017.

[10] Y. Wu, Y. Xu, X. Zhang et al., "Experimental study on vacuum preloading consolidation of landfill sludge conditioned by Fenton's reagent under varying filter pore size," *Geotextiles and Geomembranes*, vol. 49, no. 1, pp. 109–121, 2021.

[11] C. Zhu, M. He, M. Karakus, X. Cui, and Z. Tao, "Investigating toppling failure mechanism of anti-dip layered slope due to excavation by physical modelling," *Rock Mechanics and Rock Engineering*, vol. 53, pp. 5029–5050, 2020.

[12] W. Zhang, R. Zhang, C. Wu et al., "State-of-the-art review of soft computing applications in underground excavations," *Geoscience Frontiers*, vol. 11, no. 4, pp. 1095–1106, 2020.

[13] Z. Li, S. G. Liu, W. T. Ren, J. J. Fang, Q. H. Zhu, and Z. L. Dun, "Multiscale laboratory study and numerical analysis of water-weakening effect on shale," *Advances in Materials Science and Engineering*, vol. 2020, Article ID 5263431, 14 pages, 2020.

[14] Y. Wang, B. Zhang, S. H. Gao, and C. H. Li, "Investigation on the effect of freeze-thaw on fracture mode classification in marble subjected to multi-level cyclic loads," *Theoretical and Applied Fracture Mechanics*, vol. 111, article 102847, 2021.

[15] Y. Yao, J. Huang, N. Wang, T. Luo, and L. Han, "Prediction method of creep settlement considering abrupt factors," *Transportation Geotechnics*, vol. 22, article 100304, 2019.

[16] Y. Tan and D. Wang, "Characteristics of a large-scale deep foundation pit excavated by the central-island technique in Shanghai soft clay. II: top-down construction of the peripheral rectangular pit," *Journal of Geotechnical and Geoenvironmental Engineering*, vol. 139, no. 11, pp. 1894–1910, 2013.

[17] Y. Tan, W.-Z. Jiang, H.-S. Rui, Y. Lu, and D.-L. Wang, "Forensic geotechnical analyses on the 2009 building-overturning accident in Shanghai, China: beyond common recognitions," *Journal of Geotechnical and Geoenvironmental Engineering*, vol. 146, no. 7, article 05020005, 2020.

[18] Y. Tan and D. Wang, "Characteristics of a large-scale deep foundation pit excavated by the central-island technique in Shanghai soft clay. I: bottom-up construction of the central cylindrical shaft," *Journal of Geotechnical and Geoenvironmental Engineering*, vol. 139, no. 11, pp. 1875–1893, 2013.

[19] Q. Xu, H. Zhu, X. Ma et al., "A case history of shield tunnel crossing through group pile foundation of a road bridge with pile underpinning technologies in Shanghai," *Tunnelling and Underground Space Technology*, vol. 45, pp. 20–33, 2015.

[20] Q. Meng, H. Wang, M. Cai, W. Xu, X. Zhuang, and T. Rabczuk, "Three-dimensional mesoscale computational modeling of soil-rock mixtures with concave particles," *Engineering Geology*, vol. 277, article 105802, 2020.

[21] Z. Tao, C. Zhu, M. He, and M. Karakus, "A physical modeling-based study on the control mechanisms of negative Poisson's ratio anchor cable on the stratified toppling deformation of anti-inclined slopes," *International Journal of Rock Mechanics and Mining Sciences*, vol. 138, article 104632, 2021.

[22] Q. X. Meng, H. L. Wang, W. Y. Xu, and Q. Zhang, "A coupling method incorporating digital image processing and discrete element method for modeling of geomaterials," *Engineering Computations*, vol. 35, no. 1, pp. 411–431, 2018.

[23] Z. F. Wang, S. L. Shen, W. C. Cheng, and Y. S. Xu, "Ground fissures in Xi'an and measures to prevent damage to the metro tunnel system due to geohazards," *Environmental Earth Sciences*, vol. 75, no. 6, article 511, 2016.

[24] X. Gao, W.-p. Tian, and Z. Zhang, "Analysis of deformation characteristics of foundation-pit excavation and circular wall," *Sustainability*, vol. 12, no. 8, article 3164, 2020.

[25] Y. Zhou and Y. Zhu, "Interaction between pile-anchor supporting structure and soil in deep excavation," *Journal of Rock and Soil Mechanics*, vol. 39, no. 9, pp. 3246–3252, 2018.

[26] Q. X. Meng, L. Yan, Y. L. Chen, and Q. Zhang, "Generation of numerical models of anisotropic columnar jointed rock mass using modified centroidal Voronoi diagrams," *Symmetry*, vol. 10, no. 11, p. 618, 2018.

[27] A. Ismail and D. S. Jeng, "Modelling load–settlement behaviour of piles using high-order neural network (HON-PILE model)," *Engineering Applications of Artificial Intelligence*, vol. 24, no. 5, pp. 813–821, 2011.

[28] A. Ghorbani and M. Firouzi Niavol, "Evaluation of induced settlements of piled rafts in the coupled static-dynamic loads using neural networks and evolutionary polynomial regression," *Applied Computational Intelligence and Soft Computing*, vol. 2017, Article ID 7487438, 23 pages, 2017.

[29] Y. Lv, T. Liu, J. Ma, S. Wei, and C. Gao, "Study on settlement prediction model of deep foundation pit in sand and pebble strata based on grey theory and BP neural network," *Arabian Journal of Geosciences*, vol. 13, no. 23, pp. 1–13, 2020.

[30] H. T. Eid and A. A. Shehada, "Estimating the elastic settlement of piled foundations on rock," *International Journal of Geomechanics*, vol. 15, no. 3, article 04014059, 2015.

[31] C. Xu, D. Yue, and C. Deng, "Hybrid GA/SIMPLS as alternative regression model in dam deformation analysis," *Engineering Applications of Artificial Intelligence*, vol. 25, no. 3, pp. 468–475, 2012.

[32] X. Guo, S. Liu, L. Wu, Y. Gao, and Y. Yang, "A multi-variable grey model with a self-memory component and its application on engineering prediction," *Engineering Applications of Artificial Intelligence*, vol. 42, pp. 82–93, 2015.

[33] M. A. Shahin, "Load–settlement modeling of axially loaded drilled shafts using CPT-based recurrent neural networks," *International Journal of Geomechanics*, vol. 14, no. 6, article 06014012, 2014.

[34] J. P. Doherty, S. Gourvenec, and F. M. Gaone, "Insights from a shallow foundation load-settlement prediction exercise," *Computers and Geotechnics*, vol. 93, pp. 269–279, 2018.

[35] F. P. Nejad and M. B. Jaksa, "Load-settlement behavior modeling of single piles using artificial neural networks and CPT data," *Computers and Geotechnics*, vol. 89, pp. 9–21, 2017.

[36] M. Cao, L. X. Pan, Y. F. Gao et al., "Neural network ensemble-based parameter sensitivity analysis in civil engineering systems," *Neural Computing and Applications*, vol. 28, no. 7, pp. 1583–1590, 2017.

[37] J. Su, Y. Xia, Y. Xu, X. Zhao, and Q. Zhang, "Settlement monitoring of a supertall building using the Kalman filtering technique and forward construction stage analysis," *Advances in Structural Engineering*, vol. 17, no. 6, pp. 881–893, 2014.

[38] W. Dai, N. Liu, R. Santerre, and J. Pan, "Dam deformation monitoring data analysis using space-time Kalman filter," *International Journal of Geo-Information*, vol. 5, no. 12, p. 236, 2016.

[39] L. Zhang, X. Wu, W. Ji, and S. M. AbouRizk, "Intelligent approach to estimation of tunnel-induced ground settlement using wavelet packet and support vector machines," *Journal of Computing in Civil Engineering*, vol. 31, no. 2, article 04016053, 2017.

[40] C. Zhang, J.-z. Li, and H. Yong, "Application of optimized grey discrete Verhulst–BP neural network model in settlement prediction of foundation pit," *Environmental Earth Sciences*, vol. 78, no. 15, article 441, 2019.

[41] M. Guoxiong and Zai, "Proof and application of s-shape settlement-time curve for linear or nearly linear loadings," *China Civil Engineering Journal*, vol. 38, pp. 69–72, 2005.

[42] Wilun and Zenon, *Soil Mechanics in Foundation Engineering: v.2: Theory and Practice*, John Wiley, 1972.

[43] L. Tang and Y. Lu, "Study of the grey Verhulst model based on the weighted least square method," *Physica A: Statistical Mechanics and its Applications*, vol. 545, article 123615, 2020.

[44] H. Liu, W. Guo, C. Zhang, and H. Yang, "Research on the grey Verhulst model based on particle swarm optimization and Markov chain to predict the settlement of high fill subgrade in Xiangli expressway," *Mathematical Problems in Engineering*, vol. 2019, Article ID 1878296, 10 pages, 2019.

[45] B. Zeng, X. Ma, and M. Zhou, "A new-structure grey Verhulst model for China's tight gas production forecasting," *Applied Soft Computing*, vol. 96, article 106600, 2020.

[46] Q. Ma, S. Liu, X. Fan, C. Chai, Y. Wang, and K. Yang, "A time series prediction model of foundation pit deformation based on empirical wavelet transform and NARX network," *Mathematics*, vol. 8, no. 9, article 1535, 2020.

[47] T. Niu, L. Zhang, S. Wei, B. Zhang, and B. Zhang, "Study on a combined prediction method based on BP neural network and improved Verhulst model," *Systems Science & Control Engineering*, vol. 7, no. 3, pp. 36–42, 2019.

[48] J. Wang, Y. Gao, and J. Jin, "Influence of sample length on gray fuzzy prediction performance," *Journal of Intelligent & Fuzzy Systems*, vol. 38, no. 6, pp. 6745–6754, 2020.

[49] I. A. Basheer and M. Hajmeer, "Artificial neural networks: fundamentals, computing, design, and application," *Journal of Microbiological Methods*, vol. 43, no. 1, pp. 3–31, 2000.

[50] H. Peng, H. Wu, J. Wang, and T. Dede, "Research on the prediction of the water demand of construction engineering based on the BP neural network," *Advances in Civil Engineering*, vol. 2020, Article ID 8868817, 11 pages, 2020.

[51] S. M. Bateni, D.-S. Jeng, and S. M. Naeini, "Estimating soil thermal properties from sequences of land surface temperature using hybrid genetic algorithm–finite difference method," *Engineering Applications of Artificial Intelligence*, vol. 25, no. 7, pp. 1425–1436, 2012.

[52] V. Gitifar, A. Abbasi, P. Setoodeh, M. Poursadegh, Z. Sahebnazar, and A. Alamdari, "Modeling and analysis of the thermal conductivities of air saturated sandstone, quartz and limestone using computational intelligence," *International Journal of Thermal Sciences*, vol. 83, pp. 45–55, 2014.

[53] J. R. Sampson, "Adaptation in natural and artificial systems," in *Society for Industrial and Applied Mathematics*, J. H. Holland, Ed., SIAM Review, 1976.

[54] D. E. Goldberg and J. H. Holland, *Genetic Algorithms and Machine Learning*, vol. 3, pp. 95–99, Machine Learning, 1988.

[55] Y. Erzin and T. O. Gul, "The use of neural networks for the prediction of the settlement of one-way footings on cohesionless soils based on standard penetration test," *Neural Computing and Applications*, vol. 24, no. 3-4, pp. 891–900, 2014.

[56] S. Freitag, B. Cao, J. Ninić, and G. Meschke, "Recurrent neural networks and proper orthogonal decomposition with interval data for real-time predictions of mechanised tunnelling processes," *Computers & Structures*, vol. 207, pp. 258–273, 2018.

[57] Z. W. Ji, B. Wang, S. P. Deng, and Z. H. You, "Predicting dynamic deformation of retaining structure by LSSVR-based time series method," *Neurocomputing*, vol. 137, pp. 165–172, 2014.

[58] C. Zhang, Z. Peng, and W. Peng, "Application of optimized grey discrete Verhulst model in settlement prediction of foundation pit," *Journal of Central South University (Science and Technology)*, vol. 48, no. 11, pp. 3030–3036, 2017.

[59] E. Kayacan, B. Ulutas, and O. Kaynak, "Grey system theory-based models in time series prediction," *Expert Systems with Applications*, vol. 37, no. 2, pp. 1784–1789, 2010.

[60] Y. Zhang, "Improved grey derivative of grey Verhulst model and its application," *International journal of computer science Issues (IJCSI)*, vol. 9, 2012.

[61] X. Wang, L. Qi, C. Chen, J. Tang, and M. Jiang, "Grey system theory based prediction for topic trend on Internet," *Engineering Applications of Artificial Intelligence*, vol. 29, pp. 191–200, 2014.

[62] S. Ding, Y. Dang, N. Xu, D. Chen, and J. Cui, "The optimization of grey Verhulst model and its application," *The Journal of Grey System*, vol. 27, no. 2, pp. 1–13, 2015.